FULL PAPERS

Magnetic Resonance in Medicine 000:000–000 (2010)

Immobilized Contrast-Enhanced MRI: Gadolinium-Based Long-Term MR Contrast Enhancement of the Vein Graft Vessel Wall

Dimitris Mitsouras,[1,2]* Praveen Kumar Vemula,[2–4] Peng Yu,[2,5] Ming Tao,[2,5] Binh T. Nguyen,[2,5] Christina M. Campagna,[5] Jeffrey M. Karp,[2–4] Robert V. Mulkern,[1,2,6] C. Keith Ozaki,[2,5] and Frank J. Rybicki[1,2]

An implantable MR contrast agent that can be covalently immobilized on tissue during surgery has been developed. The rationale is that a durable increase in tissue contrast using an implantable contrast agent can enhance postsurgical tissue differentiation using MRI. For small-vessel (e.g., vein graft) MRI, the direct benefit of such permanent "labeling" of the vessel wall by modification of its relaxation properties is to achieve more efficient imaging. This efficiency can be realized as either increased contrast leading to more accurate delineation of vessel wall and lesion tissue boundaries, or, faster imaging without penalizing contrast-to-noise ratio, or a combination thereof. We demonstrate, for the first time, stable long-term MRI enhancement using such an exogenous contrast mechanism based on immobilizing a modified diethylenetriaminepentaacetic acid gadolinium^{3+} dihydrogen complex on a human vein using a covalent amide bond. Signal enhancement due to the covalently immobilized contrast agent is demonstrated for excised human vein specimens imaged at 3 T, and its long-term stability is demonstrated during a 4-month incubation period. Magn Reson Med 000:000–000, 2010.

Key words: high-resolution MRI; gadolinium contrast agent; targeted contrast agent; covalent amide bond; contrast enhanced imaging; vein graft imaging; vessel wall imaging

Autologous vein bypass remains the standard evidence-based treatment for selected patients with peripheral artery disease or coronary occlusive disease. Recent data reveal that within the first year almost 40% of lower extremity vein bypass grafts develop occlusive lesions or fail (1), and almost half of cardiac bypass patients will lose a vein graft (≥75% stenosis) (2). These failures result in recurrent end-organ ischemia, redo-revascularizations, and, not infrequently, loss of human limb or life.

While there is evidence linking luminal intimal hyperplasia, historically viewed as the primary etiology of vein graft failure, to a multitude of biologic pathways, reductionistic approaches focused only on specific molecular strategies have failed to demonstrate substantial impact on graft failure rates (1–4). Emerging data support an important role for negative full vessel wall remodeling (5,6) in addition to intimal hyperplasia signaling mechanisms (4), yet clinicians and researchers currently lack the ability to temporally interrogate the in vivo vein graft wall anatomy efficiently. Duplex ultrasonography, the current clinical standard-of-care for lower extremity vein grafts, detects increased blood velocities due to lumen narrowing, a result of late, severe disease (7) but lacks the resolution to provide useful information regarding the morphology of the graft wall.

We have recently demonstrated that very high-resolution T_1-weighted (T1W) MR images consistently delineate the full graft wall in vivo, and, in conjunction with T_2-weighted images, can be used to separately delineate the media and neointima from the adventitia (8). We have also demonstrated the ability of MRI to assess remodeling of those wall components at follow up (9). To achieve multicontrast imaging with sufficiently high resolutions (≤0.2 mm^3 voxel volumes) and sufficient signal-to-noise ratio (SNR) at clinically available magnetic field strengths, we (10) and other groups (11) have employed state-of-the-art high sampling efficiency fast spin echo pulse sequences.

While future enhancements in pulse sequence technologies remain highly promising for research focused on studying the biology of vein graft adaptation and failure in vivo, high spatial resolution MRI technologies remain inadequate for large-scale clinical application in patients after coronary and lower extremity graft bypass surgery. Two main limitations must be overcome for these applications. The first is the tradeoff between scan time and craniocaudal coverage. Our approach to date for sub-0.2 mm^3 human in vivo cardiac-gated black-blood vessel wall imaging relies on reduced field-of-view imaging (12–15), coupled with high sampling efficiency sequences. This

[1]Department of Radiology, Brigham and Women's Hospital, Boston, Massachusetts, USA.

[2]Harvard Medical School, Boston, Massachusetts, USA.

[3]Harvard Stem Cell Institute, Harvard University, Boston, Massachusetts, USA.

[4]Harvard-MIT Division of Health Science and Technology, Department of Medicine, Brigham and Women's Hospital, Boston, Massachusetts, USA.

[5]Department of Surgery, Brigham and Women's Hospital, Boston, Massachusetts, USA.

[6]Department of Radiology, Children's Hospital, Boston, Massachusetts, USA.

Grant sponsor: NIH; Grant numbers: R01HL079135, T32HL007734, R01HL095722, K23EB882; Grant sponsor: American Heart Association; Grant number: 0970178N; Grant sponsor: Ewing Marion Kauffman Foundation for Entrepreneur.

*Correspondence to: Dimitris Mitsouras, Ph.D., Brigham and Women's Hospital, Applied Imaging Science Laboratory, Department of Radiology, 75 Francis St, Boston, MA 02115. E-mail: dmitsouras@alum.mit.edu

Received 31 January 2010; revised 20 July 2010; accepted 23 July 2010.

DOI 10.1002/mrm.22606

Published online in Wiley Online Library (wileyonlinelibrary.com).

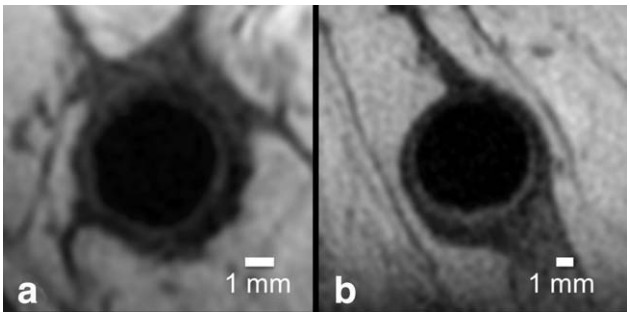

FIG. 1. Example 1.5 T in vivo black blood T1W 3D fast spin echo images (16 msec echo time, 1 R-R TR, ±16 kHz bandwidth, 12 ETL, four signal averages; 0.3 × 0.3 mm^2 resolution, 2 mm section thickness) of lower extremity vein grafts at 6 (**a**) and 1 (**b**) months post implantation. The thin vein graft wall can be delineated except at interfaces with tissues possessing similar signal intensity, such as scar tissue.

allows us to image a 3.6 cm peripheral vein graft segment at 1.5 T (14.4 cm at 3 T) during a 10-min acquisition (10) by concentrating scan time to resolving only the vessel and its immediate surroundings. While useful for characterizing focal lesions in vivo over time (4), this is insufficient for clinical surveillance of a typical lower extremity graft that extends between 40 and 80 cm in length. The second limitation that must be addressed is that of accurate discrimination between the vessel wall and adjacent tissues with similar relaxation rates and signal intensities, such as muscle, scar tissue, and edema in certain instances (Fig. 1).

This work develops and evaluates an exogenous MR contrast mechanism that can be introduced at the time of surgery to address these two limitations. We recently demonstrated the feasibility of using ultrasmall paramagnetic iron oxide nanoparticles modified to covalently bind to tissue as a strategy to enhance vein graft wall imaging (16). Because of magnetic susceptibility, these particles induce an MR signal void between the vein adventitia and surrounding tissue, enhancing delineation of the vein wall from surrounding tissue and addressing the latter limitation of MRI for this application.

Here we develop and demonstrate an implantable gadolinium (Gd)-based contrast agent to address both limitations. Unlike ultrasmall paramagnetic iron oxide particles, a Gd-based agent stands to not only enhance the contrast differential between the vein and surrounding tissues but also additionally increase the MR signal emanating from the entire vessel wall at desirable T_1 contrast weightings. An increase in T1W signal can be traded for faster imaging while maintaining the same SNR for the vessel wall tissue as that obtained in an unenhanced vessel (8). This can be accomplished with, for example, reduced signal averaging and homodyne ("half-Fourier") detection, introduction of parallel imaging, decreased pulse repetition time (TR), etc.

This work is divided into two parts. First, we demonstrate that the implantable Gd-based complex can be covalently immobilized on the human vein wall and selectively modify its relaxation properties. Second, we demonstrate the long-term stability of the crosslink via longitudinal assessment of those relaxation properties.

MATERIALS AND METHODS

Activation of Diethylenetriaminepentaacetic acid Gd^{3+} dihydrogen for Immobilization

The immobilization of diethylenetriaminepentaacetic acid Gd^{3+} dihydrogen (Gd-DTPA) complex on tissue was based on *N*-hydroxysuccinamide (NHS) ester coupling chemistry (17). NHS esters are reactive groups that under physiological conditions react with primary amines (NH_2), such as those found on the surface of cells, to form a covalent amide bond. Importantly, this approach does not compromise inherent cell properties such as viability, adhesion kinetics, and proliferation (17). The process of preparing Gd chelates for covalent binding to amines involves a reaction wherein free carboxylic acid groups in the Gd-DTPA complex are first coupled with NHS using *N,N′*-diisopropylcarbodiimide (DIC, c.f., Fig. 2) by dissolving a desired concentration of Gd-DTPA in double-distilled water, adding NHS and dimethyl sulfoxide containing DIC at twice the concentration, and incubating for a period of time at room temperature. Incubation lasted either 3 h or overnight under continuous stirring, as noted for individual experiments. The resulting solution contains "activated" Gd-DTPA molecules that possess NHS-ester groups (Fig. 2).

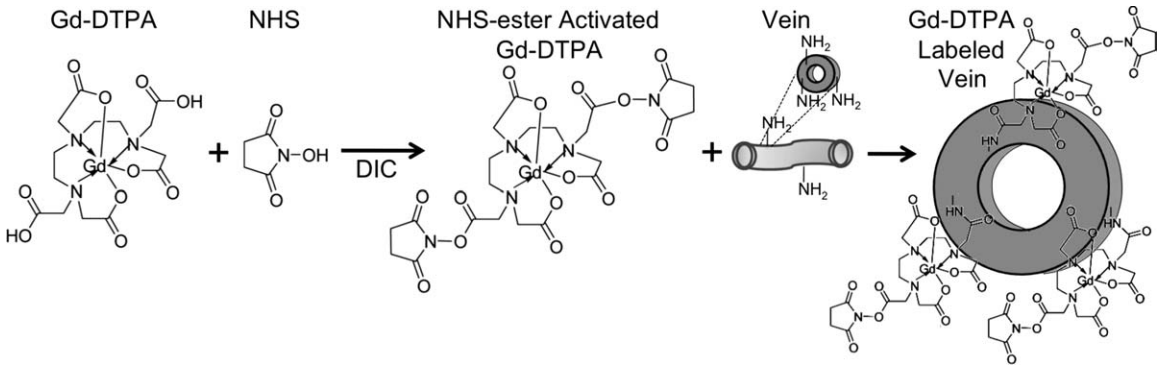

FIG. 2. Activation of carboxylic acid groups of the Gd-DTPA complex using *N*-hydroxysuccinamide chemistry to enable crosslinking to tissue. The activated ester reacts with primary amines (—NH_2) at physiological conditions to form a covalent amide bond, permanently "immobilizing" the activated Gd-DTPA onto the tissue.

Tissue Labeling With Activated Gd-DTPA

Veins were "labeled" with the activated Gd-DTPA by incubating for 30 min at room temperature in a phosphate buffered saline (PBS) solution (pH 7.4) containing the activated Gd-DTPA. Ligatures were placed on both vein ends before treatment so as to reduce endothelium exposure to the contrast agent. Following this labeling process, excess PBS was removed, and vein segments were thoroughly soaked and rinsed thrice with fresh PBS to remove nonbound Gd-DTPA.

Specimens

The institutional human research committee approved this study. Four fresh human saphenous vein specimens were harvested from discarded operating room tissue. Two were obtained from a below knee amputation, and two from a bypass surgery. Specimens were prepared for imaging immediately after harvesting.

Specimen Preparation

One specimen was used to confirm the presence of Gd using scanning electron microscopy and elemental mapping as described below. The specimen was separated into treatment and control halves. The control half was incubated in PBS, while the treatment half was labeled in 10 mmol L^{-1} (mM) solution of the activated Gd-DTPA complex that had undergone the 3 h preparation. To simulate in vivo black-blood T1W imaging (10,12), both segments were distended to physiologic arterial pressure using corn oil and MR imaging used a fat resonance-selective saturation pulse.

Two specimens were used to obtain more direct evidence of immobilization of the activated Gd-DTPA onto vein wall tissue. One specimen was used to verify that MR image enhancement and longitudinal (R_1) and transverse (R_2) relaxation rate changes were present for tissue treated with activated Gd-DTPA and absent for tissue treated with standard Gd-DTPA. The specimen was separated into five segments, with one control, three segments labeled in 1, 2.5, and 5 mM of activated Gd-DTPA solution prepared using the overnight protocol, and one segment undergoing the same incubation process as the three labeled segments except that the solution contained 5 mM of standard Gd-DTPA (i.e., without activation by NHS ester). A second specimen was used to verify the observed relationship between tissue relaxation rates and treatment concentration. That specimen was separated into six segments, with one used as a control and the remaining five labeled in 1, 2, 4, 6, and 10 mM of activated Gd-DTPA solution prepared using the overnight protocol.

Finally, one specimen was used to study the long-term stability of the immobilized Gd-DTPA. The specimen was separated into two segments, with one half used as a control and the other half labeled in 10 mM solution of activated Gd-DTPA prepared using the 3-h protocol. Sodium azide, a preservative that prevents tissue spoilage (18), was subsequently added to the saline used in the imaging setup (vide infra), and the specimen was incubated in a shaker over 4 months at 37°C to simulate in vivo conditions. R_1 and R_2 rates were measured at 0 and 122 days following harvest. The R_2 rate was additionally measured at 22 days.

Specimen Preparation for Imaging

To avoid collapse of the thin-walled veins for imaging and to simulate the in vivo signal environment, the ends of vein segments were surgically tied and either saline or corn oil as pertaining to each experiment was used to distend them to 80 mmHg. Distended veins were then suspended in saline-filled Petri dishes with the use of two 2.5 mm polystyrene struts. Prepared Petri dishes were sealed using surgical tape. With the exception of the long-term stability experiment, specimens were stored at 4°C for no longer than 12 h between preparation and imaging. To avoid cross contamination, each vein segment for each experiment was handled with separate surgical instruments and mounted in a separate Petri dish.

MRI Equipment

All experiments were performed on a 3 T GE HDx MR imager (General Electric, Milwaukee, WI), equipped with 40 mT m^{-1}, 150 T m^{-1} sec^{-1} gradients. A wrist extremity bird-cage transmit/receive coil was used for radiofrequency excitation and signal reception.

MR Imaging

MR image enhancement was assessed in three-dimensional (3D) spoiled gradient recalled echo T1W images (4 msec echo time, 30 msec TR, 40° flip angle (FA), ±32 kHz bandwidth). The SNR was measured for each vein segment as $\mathrm{SNR} = \frac{S_{\mathrm{tissue}}}{\sigma_{\mathrm{image}}}$, where S_{tissue} the mean signal intensity in a region-of-interest (ROI) containing vein wall tissue, and where the standard deviation of noise in the image was calculated as $\sigma_{\mathrm{image}} = S_{\mathrm{noise}}/\sqrt{\pi/2}$ with S_{noise} the mean signal intensity in a ROI containing air (19). SNR measurements are reported as the mean and standard deviation over multiple ROIs for each vein segment.

Environmental Scanning Electron Microscope–Energy-Dispersive X-Ray Imaging

An environmental scanning electron microscope (FEI/Philips XL30 FEG-ESEM, FEI, Hillsboro, Oregon) equipped with an energy-dispersive X-ray (EDAX) spectrometry module (Torr Scientific Ltd., UK) was used to obtain micrographs of 4-μm-thick sections of one specimen at 10 kV. Elemental mapping analysis to identify the presence of Gd was performed using the EDAX technique in which characteristic X-rays emitted from the sample after electron bombardment are used to identify element-specific signatures. Combined with environmental scanning electron microscope, spectra analyzed in a raster fashion produce a two-dimensional image of the spatial distribution of Gd.

Quantitative MR Relaxation Rate Measurements

For the long-term stability specimen, R_2 was measured using a multiecho two-dimensional Carr-Purcell-Meiboom-Gill sequence (20). A 3D Carr-Purcell-Meiboom-Gill sequence (8) with composite (90_x–180_y–90_x) refocusing pulses (21) was used to measure the R_2 of specimens with multiple labeling concentrations. The increased SNR and reduced indirect and stimulated echoes at longer echo train lengths (ETL) afford the latter sequence enhanced accuracy for graded R_2 comparisons. For two-dimensional Carr-Purcell-Meiboom-Gill, images were acquired at eight echo times (11 msec echo spacing, 1500 msec TR). For 3D Carr-Purcell-Meiboom-Gill, images were produced at 16 echo times (11.6 msec echo spacing, 1600 msec TR).

R_1 was measured using a high sampling efficiency 3D fast spin echo (eight ETL, 7 msec echo spacing) (15) with an 8.64 msec adiabatic inversion recovery preparatory pulse. For the long-term stability experiment, images were obtained at five inversion times ranging from 50 to 1000 msec at 250-msec intervals, with a TR of 1800 msec. For the two experiments with multiple concentrations, images were obtained at 11 inversion times, with eight inversion times between 125 and 1000 msec at 125-msec intervals and three additional inversion times at 50, 1250, and 1500 msec, with a TR of 3000 msec.

Relaxation rates were obtained by fitting signal intensities in ROIs using an idealized signal model; R_2 rates were obtained by fitting to the model $s(t) = \alpha e^{-tR_2}$, where t is the echo time and α is a constant reflecting the spin density. R_1 rates were obtained by fitting to the model, $s(t) = \alpha\left(1 - (1-k)e^{-t\cdot R_1} - ke^{-TR\cdot R_1}\right)$, where t is the inversion time, α as mentioned above, and $-1 \leq k \leq 1$, a constant accounting for the efficiency of the inversion pulse (22). Fitting was performed with a nonlinear optimization routine (MATLAB R2008b, MathWorks, Natick, MA) employing a non-negativity constraint for each fitted variable. Mean relaxation rates are reported by averaging fits from no less than twenty ROIs per vein segment.

Statistical Analysis

For the experiment with segments incubated in both activated and nonactivated Gd-DTPA, one-way analysis of variance of the R_1 and R_2 rates was used to test whether segments labeled with activated Gd-DTPA had significantly different relaxation rates than the control segment and the segment incubated in standard Gd-DTPA. A P value less than 0.05 was considered significant, indicating a significantly different mean relaxation rate compared with the control due to the presence of Gd-DTPA.

For the two experiments with multiple concentrations of activated Gd-DTPA, linear regression was used to determine the relationship between the treatment agent concentration and tissue R_1 and R_2 rates, and to subsequently determine the ratio of r_2 to r_1 relaxivity of the agent. Specifically, we begin by defining the "pseudo-relaxivities" r'_i, $i = 1,2$, of the agent as the regression coefficients of the models $R_i = R_i^0 + r'_i \times C_{\text{treatment}}$, $i = 1,2$, where R_i^0 is the tissue relaxation rate in the absence of contrast agent, and $C_{\text{treatment}}$ the treatment concentration of activated Gd-DTPA. A Pearson correlation coefficient $r \geq 0.9$ was considered indicative of no saturation of the available binding sites on the tissue having occurred for the particular reaction conditions. In this event, one may assume that the treatment concentration is directly proportional to the resulting tissue concentration, up to a constant factor related to each particular specimen's uptake rate for the incubation conditions. That is, we can infer that the relationship $C_{\text{tissue}} = \alpha C_{\text{treatment}}$ holds for some constant α specific to each individual experiment. Consequently, the ratio of r_2 to r_1 relaxivity of the implanted agent can be computed from the observed pseudo-relaxivities, r'_1, as the constant drops out.

For the long-term stability experiment, we first tested whether relaxation rates differed between labeled and control segments at each individual time point using the unpaired two-tailed student t-test. A P value less than 0.05 was considered significant, indicating a significantly different mean relaxation rate for the labeled versus control segments of the veins due to the presence of Gd-DTPA. Second, we tested whether the relaxation rate of each segment differed between time points. Analysis of variance was used to perform this comparison across the three time points where R_2 was measured, and the unpaired two-tailed student t-test was used for the equivalent comparison of R_1 rates, as those were only measured at two time points. In either case, a P value greater than 0.05 was considered indicative of no significant change in the mean relaxation rate of the particular vein segment over the experiment duration.

RESULTS

Labeled vein segments presented significantly higher T1W signal intensity than controls (Figs. 3–4), with SNR between 1.5 and 4.5 times higher for labeled than for control vein segments. EDAX confirmed the presence of Gd on the labeled vein segment only (Fig. 3), concentrated primarily on the outer surface of the adventitia. However, Gd ions were observed diffusely throughout the vessel wall, in agreement with all MR image results that showed increased signal intensity throughout the wall (Figs. 3–5). The signal intensity of surrounding saline did not differ between the labeled and control segments in any experiments, indicating absence of free Gd-DTPA at the time of imaging.

The increased T1W signal and positive EDAX finding offer preliminary confirmation that the activated Gd-DTPA complex can selectively enhance the relaxation properties of the target tissue. Evidence supporting immobilization onto tissue constituents follows more directly from the experiments portrayed in Figs. 4 and 5. Specifically, the R_1 and R_2 rates of a vein incubated in 5 mM of nonactivated Gd-DTPA were no different than those of the control (R_2: 10.5 ± 0.8 s^{-1} treated versus 10.6 ± 1.0 s^{-1} control, $P = 0.561$; R_1: 0.89 ± 0.03 s^{-1} treated versus 0.87 ± 0.07 s^{-1} control, $P = 0.102$, Fig. 4), confirming that vein wall tissue did not retain any significant amount of nonactivated Gd-DTPA. In contrast, all segments of that vein incubated in activated Gd-DTPA presented significantly higher relaxation rates (R_2: 13.7

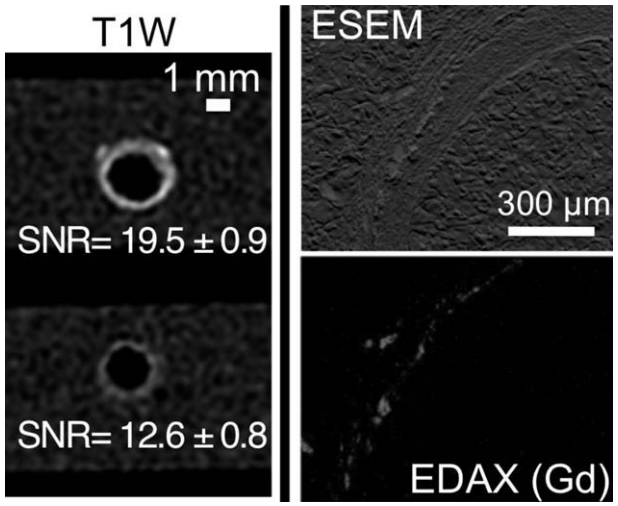

FIG. 3. Left hand panel: 3D spoiled gradient recalled echo T1W images of saphenous vein labeled with activated Gd-DTPA as described in text (top row) versus untreated control vein (bottom row). Veins are distended to physiologic pressure using corn oil to simulate black-blood imaging. Right hand panel: Environmental scanning electron microscope micrograph and EDAX elemental mapping (see text for details) of the labeled vein confirming the presence of Gd; the untreated control (not shown) indicated no presence of Gd.

$\pm$ 0.8 s^{-1}, 17.8 $\pm$ 1.5 s^{-1}, and 24.1 $\pm$ 2.4 s^{-1} for 1, 2.5, and 5 mM, respectively, $P < 0.001$ versus control; R_1: 1.29 $\pm$ 0.16 s^{-1}, 2.12 $\pm$ 0.26 s^{-1}, and 3.58 $\pm$ 0.28 s^{-1} for 1, 2.5, and 5 mM, respectively, $P < 0.001$ versus control), confirming the presence of Gd. This strongly suggests successful implantation of only activated Gd-DTPA onto the vein wall tissue and clarifies that in the absence of NHS-ester activation, surface interactions between Gd-DTPA and the vein wall tissue are limited.

Additional information regarding the particular nature of the interaction between activated Gd-DTPA and vein tissue can be obtained from the rate of change of the relaxation rates with respect to the concentration of the implanted agent. The observed relationship between relaxation rate and incubation concentration was highly linear for both $R_{1,2}$ (Pearson $r > 0.95$ for all fits, Fig. 5) over the tested range of 0–10 mM. Consequently, we infer that the number of binding sites on the vein tissue was not saturated, and that the tissue concentrations achieved were directly proportional to the treatment concentration up to a multiplicative factor specific to each particular specimen. Using the pseudo-relativities (slopes of the fitted models) under this linearity assumption, the ratio of r_2 to r_1 relaxivity of the activated Gd-DTPA is calculated to be 4.81 $\pm$ 0.18 and 4.89 $\pm$ 0.36 in these two experiments.

Finally, the crosslinkage of Gd-DTPA to vein wall tissue was stable over a 4-month period; both R_1 and R_2 rates remained stable throughout this period for both the control ($P > 0.250$, Fig. 6) and the labeled ($P > 0.159$, Fig. 6) vein segments. Labeled segment R_2 ranged from 14.66 $\pm$ 1.61 s^{-1} at harvest to 14.96 $\pm$ 1.43 s^{-1} at 122 days, and was significantly higher than that of the control (9.06 $\pm$ 1.35 s^{-1} at harvest to 8.45 $\pm$ 1.00 s^{-1} at 122 days) at all three time points ($P < 0.001$, Fig. 6). R_1 was also significantly different between the control and labeled segments at both time points ($P < 0.001$, Fig. 6); the labeled segment's R_1 was 1.56 $\pm$ 0.12 s^{-1} at harvest

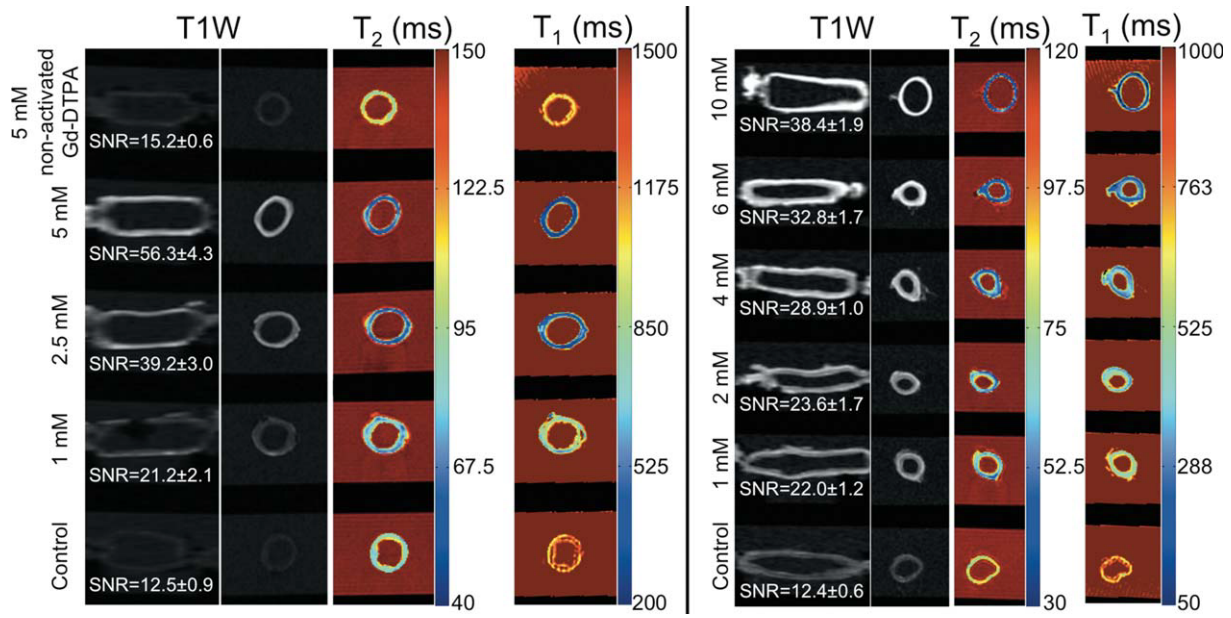

FIG. 4. Three-dimensional spoiled gradient recalled echo T1W images and $T_{1,2}$ relaxation times of veins incubated in varying concentrations of activated and nonactivated (standard) Gd-DTPA. Left panel: specimen with segments incubated in (top to bottom) 5 mM standard, 5, 2.5, and 1 mM of activated Gd-DTPA, and untreated control. Right panel: specimen with segments incubated in (top to bottom:) 10, 6, 4, 2, and 1 mM activated Gd-DTPA, and untreated control. Graded increase in T1W signal intensity and reduction of $T_{1,2}$ are observed with increasing treatment concentration for all segments. Segment incubated in 5 mM standard Gd-DTPA demonstrates significantly smaller differences compared to control.

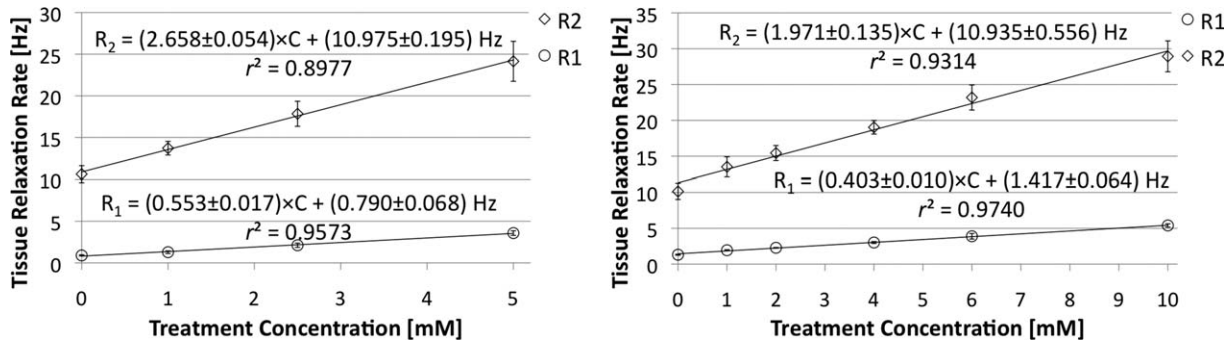

FIG. 5. Transverse and longitudinal relaxation rates of two specimens with segments treated in different concentrations of activated Gd-DTPA (c.f., Fig 4). Highly linear relationships indicate that the tissue concentration achieved for each specimen was proportional to the treatment concentration, up to a constant factor. The ratio of r_2 to r_1 relaxivity of the agent is computed from the fitted pseudo-relaxivities ($r'_{1,2}$) , and equals 4.81 ± 0.18 and 4.89 ± 0.36 for these specimens, indicative of a reduced tumbling rate for the Gd complex as would be expected due to its covalent immobilization onto large tissue constituents.

and 1.52 ± 0.09 s^{-1} at 122 days, compared to 0.86 ± 0.05 s^{-1} at harvest and 0.89 ± 0.11 s^{-1} at 122 days for the control.

DISCUSSION

Postintervention MRI represents a large fraction of clinical scanning. The separation of recurrent disease from surrounding tissues can often be more difficult than the initial detection of an abnormality because the tissues are altered, potentially decreasing contrast between them, e.g., due to edema or scar. In vessel wall imaging, contrast optimization is critical for the reproducibility of wall area measurements (23). The importance of assessing wall tissue volume rather than lumen loss is underscored by the fact that atherosclerotic plaque burden may increase without significant lumen narrowing (24). Similarly, in bypass grafts loss of patency can be a result of not only intimal hyperplasia encroaching into the lumen but of full conduit negative remodeling as well (4–6). To observe the early events in the vessel wall that culminate to these highly focal failures requires repeated surveillance of the full 40–80 cm craniocaudal extent of a typical vein graft. This is currently unattainable in a clinical setting given the high spatial resolutions required (10).

The possibility of conjugating Gd chelates to macromolecules, using covalent or noncovalent bonds, has long been recognized (25,26). Aside from enhancing the relaxivity of the metal complex by reducing its tumbling rate (25–29), additional benefits can be obtained, such as retention of the agent within the blood pool for significantly longer periods than for nonconjugated agents (28), or, targeting to a specific pathology such as necrotic tissue in myocardial infarction (30).

Here, we postulated that a Gd-based agent might be indiscriminately targeted and permanently attached (i.e., implanted) to surgically exposed tissue, in order to achieve durable, long-term signal enhancement that is biologically well tolerated (17). To this end, a modified Gd-DTPA complex was developed that crosslinks to tissue via a covalent amide bond. The small molecular weight of Gd-DTPA (cation molecular weight = 547 daltons) allows it to quickly enter the interstitial space (25) and enhance the entirety of vessel wall tissue (31). When a vein is incubated with the activated Gd chelate, one might similarly expect that the complex readily permeates the fibrous adventitial layer through the vasa vasorum, subsequently reacting with amines found deeper within the tissue constituents to effectively become permanently "immobilized" there.

Our results show that such "immobilized contrast-enhanced" MRI is a valid proposition that can be realized

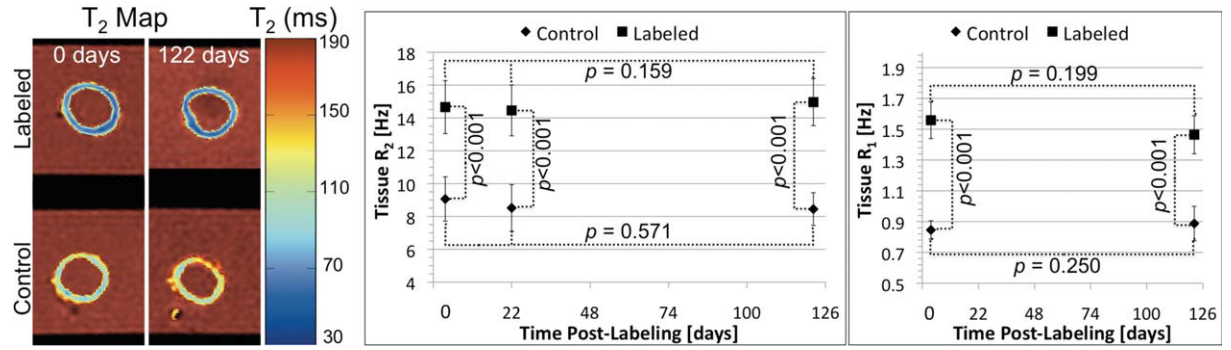

FIG. 6. Left panel: T_2 maps of a vein segment labeled with the implantable Gd-DTPA contrast agent and an untreated control at zero and 122 days postimplantation. Right panel: mean R_2 and R_1 rates for each segment across time points indicate no loss of immobilized contrast agent, but a persistent significant difference between labeled and control segments.

for significant gains. The 1.5- to 4.5-fold increase in T1W SNR observed *in vitro* can be readily traded for a 2- to 20-fold increase in T1W imaging speed while maintaining the SNR, spatial resolution, and contrast-to-noise ratio (CNR) expected for unenhanced tissue. For lower extremity vein bypass grafts, where the full vessel wall can be delineated in T1W images (8), a 4-fold reduction in imaging time that can be realized by a 2-fold increase in SNR—well within the SNR increases demonstrated here—would immediately enable us to extend in vivo surveillance to the entire graft in the same scan time as we currently use for only a short segment (8,10).

Before further exploring the use of this implantable contrast agent for such longitudinal surveillance applications it is important to ensure that it leads to contrast enhancement that (a) is specific to the tissue it is implanted on, (b) it possesses a robust relationship with labeling treatment conditions, and (c) can be maintained over a significant period of time.

Regarding the first requirement, our results demonstrate that the implantable Gd-DTPA attaches to the target tissue, as opposed to being temporarily absorbed. Only veins treated with activated Gd-DTPA presented increased relaxation rates compared to control, while a segment treated with standard (unactivated) Gd-DTPA under otherwise identical conditions presented no significant differences. Another feature of the data that lends credence to the theory that the activated Gd-DTPA binds with the tissue is that its r_2 relaxivity was nearly five times larger than its r_1 relaxivity (c.f., Fig. 5). Preferential R_2 enhancement is characteristic of increased low-frequency fluctuations associated with Gd ions attached onto large molecular weight compounds. According to standard Bloembergen, Pound, and Purcell theory, longitudinal relaxation rates are most sensitive to random magnetic field fluctuations at, and near, the Larmor frequency and twice the Larmor frequency, while transverse relaxation rates are additionally sensitive to very low DC frequency fluctuations (32). A dramatic reduction in tumbling frequency, as achieved by bonding Gd chelates to e.g., human albumin for MS-325 (28,33), and as perhaps afforded by anchoring Gd-DTPA to solid vein wall tissue constituents in this study, preferentially enhances transverse over longitudinal relaxation as only the latter is sensitive to very low frequency magnetic fluctuations.

The relationship between treatment conditions and signal enhancement, i.e., the "bang for the buck," as it were, is a multifaceted issue. It is affected by the agent tissue concentration achievable, tissue composition, as well as the relaxivities of the agent, which are in turn affected by the crosslinkage. The tissue concentration that can be successfully implanted depends not only on the concentration of agent used in the labeling reaction but also on the number of available binding sites (free primary amines) on the exposed tissue surfaces. The former appears to have been a limitation in our early experiments; the 3-h Gd-DTPA activation protocol resulted in significantly smaller differences in tissue $R_{1,2}$ at the same treatment concentration when compared with the overnight preparation. Thus, it appears that the reaction yields a significantly larger percentage of activated Gd-DTPA under constant stirring and extended duration.

The availability of binding sites may still pose a limitation, since it may vary significantly depending on the type and condition of tissue. The increased r_2 to r_1 relaxivity ratio, characteristic of immobilized Gd chelates and observed here, may exacerbate this as higher tissue concentrations, necessary to achieve further signal enhancement from T_1 effects, will ultimately be limited by the accompanying T_2 shortening. For the saphenous veins examined here, binding sites were not saturated yet the achieved tissue concentrations sufficed to impart large signal changes. The right hand panel of Fig. 4 indicates a T_1 change from 763.3 $\pm$ 43.5 msec (control) to 185.7 $\pm$ 7.9 msec (10-mM treatment), accompanied by a T_2 change from 99.8 $\pm$ 11.2 to 34.7 $\pm$ 2.7 msec. However, the resulting 3.1-fold SNR increase of that vein in a standard T1W acquisition equates to a 9-fold scan time reduction that can be readily realized using standard methods such as signal averaging reduction and parallel imaging. Overall signal increases of the order of 4.5-fold achieved in this study should suffice for most conceivable desired benefits for state-of-the-art vessel wall imaging. Nonetheless, should saturation of binding sites prove a limitation for other applications, dendrimers with multiple Gd ions per molecule (34) may be considered, since the simple crosslinking chemistry we used is readily portable to many molecules.

Regarding the final requirement, preliminary results here demonstrate the *in vitro* durability of the Gd-DTPA crosslinkage in a vein incubated for 4 months. Relaxation rate differences between a treated and an untreated vein segment stably persisted throughout the duration of the experiment, indicating reasonably long-term binding of the agent to tissue constituent. In vivo experiments, initially in an animal model, are now required to assess whether other biologic processes can affect the stability of the crosslink, the stability of complex itself [e.g., in vivo chelate dissociation, leading to free Gd ions, and transmetalation (30)], or the tissue concentration of the agent over time, as this can be affected by cell internalization via endocytosis and subsequent cell migration and proliferation. Conversely, in vivo experiments are necessary to assess whether the contrast agent affects the biologic viability and function of the vein graft and host. Nonetheless, the preliminary results reported here argue that further experimentation with the developed Gd-DTPA agent is warranted.

CONCLUSION

A novel technique was developed to provide stable long-term enhancement for MR imaging of a tissue that is implanted or altered during a surgical intervention based on a modified Gd-DTPA contrast agent. Vein bypass grafts are an important such example; veins are too small to efficiently image using non-invasive modalities. As a result, ultrasonography, and computed tomography or MR angiography are used for follow up. While these modalities are able to detect late stenoses, typically long after they become hemodynamically significant, there is no noninvasive imaging modality capable of detecting early changes that occur in the vein wall and that may culminate to these focal stenoses. We have demonstrated

that the novel implantable contrast agent developed can be covalently immobilized on the vessel wall tissue, and remain bonded to it over an extended period of time. Significant, persistent signal gains are obtained for tissue "labeled" with this contrast agent for standard T1W imaging sequences. These gains can be freely traded for faster imaging and larger craniocaudal coverage, enhanced definition of the boundaries of the labeled tissue, or any combination thereof.

ACKNOWLEDGMENTS

The authors would like to thank Prof. Frederick J. Schoen, MD, PhD for helpful discussions. This work was supported in part by NIH grants (CKO, JMK, and FJR), American Heart Association grant (JMK), and the Ewing Marion Kauffman Foundation for Entrepreneur Postdoc Fellowship (PKV).

REFERENCES

1. Conte MS, Bandyk DF, Clowes AW, Moneta GL, Seely L, Lorenz TJ, Namini H, Hamdan AD, Roddy SP, Belkin M, Berceli SA, DeMasi RJ, Samson RH, Berman SS. Results of PREVENT III: a multicenter, randomized trial of edifoligide for the prevention of vein graft failure in lower extremity bypass surgery. J Vasc Surg 2006;43:742–751; discussion 751.
2. Alexander JH, Hafley G, Harrington RA, Peterson ED, Ferguson TB, Jr., Lorenz TJ, Goyal A, Gibson M, Mack MJ, Gennevois D, Califf RM, Kouchoukos NT. Efficacy and safety of edifoligide, an E2F transcription factor decoy, for prevention of vein graft failure following coronary artery bypass graft surgery: PREVENT IV: a randomized controlled trial. JAMA 2005;294:2446–2454.
3. Jiang Z, Shukla A, Miller BL, Espino DR, Tao M, Berceli SA, Ozaki CK. Tumor necrosis factor-alpha and the early vein graft. J Vasc Surg 2007;45:169–176.
4. Owens CD. Adaptive changes in autogenous vein grafts for arterial reconstruction: clinical implications. J Vasc Surg 2009;51:736–746.
5. Kaneda H, Terashima M, Takahashi T, Iversen S, Felderhoff T, Grube E, Yock PG, Honda Y, Fitzgerald PJ. Mechanisms of lumen narrowing of saphenous vein bypass grafts 12 months after implantation: an intravascular ultrasound study. Am Heart J 2006;151:726–729.
6. Lau GT, Ridley LJ, Bannon PG, Wong LA, Trieu J, Brieger DB, Lowe HC, Freedman BS, Kritharides L. Lumen loss in the first year in saphenous vein grafts is predominantly a result of negative remodeling of the whole vessel rather than a result of changes in wall thickness. Circulation 2006;114(1 Suppl):I435–I440.
7. Rybicki FJ, Nallamshetty L, Yucel EK, Holtzman SR, Baum RA, Foley WD, Ho VB, Mammen L, Narra VR, Stein B, Moneta GL. ACR appropriateness criteria on recurrent symptoms following lower-extremity angioplasty. J Am Coll Radiol 2008;5:1176–1180.
8. Mitsouras D, Owens CD, Conte MS, Ersoy H, Creager MA, Rybicki FJ, Mulkern RV. In vivo differentiation of two vessel wall layers in lower extremity peripheral vein bypass grafts: application of high-resolution inner-volume black blood 3D FSE. Magn Reson Med 2009;62:607–615.
9. Rybicki FJ, Mitsouras D, Owens CD, Whitmore AG, Ersoy H, Mulkern RV, Creager MA, Conte MS. Lower extremity peripheral vein bypass graft wall thickness changes demonstrated at 1 and 6 months after surgery with ultra-high spatial resolution black blood inner volume three-dimensional fast spin echo magnetic resonance imaging. Int J Cardiovasc Imaging 2008;24:529–533.
10. Mitsouras D, Mulkern RV, Owens CD, Conte MS, Ersoy H, Luu TM, Whitmore AG, Creager MA, Rybicki FJ. High resolution peripheral vein bypass graft wall studies using high sampling efficiency inner volume 3D FSE. Magn Reson Med 2008;59:650–654.
11. Terry CM, Kim SE, Li L, Goodrich KC, Hadley JR, Blumenthal DK, Parker DL, Cheung AK. Longitudinal assessment of hyperplasia using magnetic resonance imaging without contrast in a porcine arteriovenous graft model. Acad Radiol 2009;16:96–107.
12. Crowe LA, Gatehouse P, Yang GZ, Mohiaddin RH, Varghese A, Charrier C, Keegan J, Firmin DN. Volume-selective 3D turbo spin echo imaging for vascular wall imaging and distensibility measurement. J Magn Reson Imaging 2003;17:572–580.
13. Feinberg DA, Hoenninger JC, Crooks LE, Kaufman L, Watts JC, Arakawa M. Inner volume MR imaging: technical concepts and their application. Radiology 1985;156:743–747.
14. Luk-Pat GT, Gold GE, Olcott EW, Hu BS, Nishimura DG. High-resolution three-dimensional in vivo imaging of atherosclerotic plaque. Magn Reson Med 1999;42:762–771.
15. Mitsouras D, Mulkern RV, Rybicki FJ. Strategies for inner volume 3D fast spin echo magnetic resonance imaging using nonselective refocusing radio frequency pulses. Med Phys 2006;33:173–186.
16. Ozaki CK, Mitsouras D, Vemula PK, Smiley D, Tao M, Yu P, Campagna C, Zhao W, Mulkern RV, Karp J, Rybicki FJ. Novel implantable vein graft contrast yields enhanced outer wall definition in magnetic resonance imaging. J Vasc Surg 2010;51:533.
17. Sarkar D, Vemula PK, Teo GS, Spelke D, Karnik R, Wee le Y, Karp JM. Chemical engineering of mesenchymal stem cells to induce a cell rolling response. Bioconjug Chem 2008;19:2105–2109.
18. Minassian H, Huang S. Effect of sodium azide on the ultrastructural preservation of tissues. J Microsc 1979;117:243–253.
19. Henkelman RM. Measurement of signal intensities in the presence of noise in MR images. Med Phys 1985;12:232–233.
20. Roebuck JR, Haker SJ, Mitsouras D, Rybicki FJ, Tempany CM, Mulkern RV. Carr-Purcell-Meiboom-Gill imaging of prostate cancer: quantitative T2 values for cancer discrimination. Magn Reson Imaging 2009;27:497–502.
21. Poon CS, Henkelman RM. Practical T2 quantitation for clinical applications. J Magn Reson Imaging 1992;2:541–553.
22. Kingsley PB, Monahan WG. Effect of increased repetition time TR on precision of inversion-recovery T(1) measurements. Magn Reson Imaging 2001;19:279–282.
23. Zhang S, Hatsukami TS, Polissar NL, Han C, Yuan C. Comparison of carotid vessel wall area measurements using three different contrast-weighted black blood MR imaging techniques. Magn Reson Imaging 2001;19:795–802.
24. Chatzizisis YS, Jonas M, Coskun AU, Beigel R, Stone BV, Maynard C, Gerrity RG, Daley W, Rogers C, Edelman ER, Feldman CL, Stone PH. Prediction of the localization of high-risk coronary atherosclerotic plaques on the basis of low endothelial shear stress: an intravascular ultrasound and histopathology natural history study. Circulation 2008;117:993–1002.
25. Brasch RC. Rationale and applications for macromolecular Gd-based contrast agents. Magn Reson Med 1991;22:282–287; discussion 300–283.
26. Lauffer RB. Targeted relaxation enhancement agents for MRI. Magn Reson Med 1991;22:339–342; discussion 343–336.
27. Lauffer RB. Paramagnetic metal complexes as water proton relaxation agents for NMR imaging: theory and design. Chem Rev 1987;87:901–927.
28. Lauffer RB, Parmelee DJ, Dunham SU, Ouellet HS, Dolan RP, Witte S, McMurry TJ, Walovitch RC. MS-325: albumin-targeted contrast agent for MR angiography. Radiology 1998;207:529–538.
29. Schmiedl U, Ogan MD, Moseley ME, Brasch RC. Comparison of the contrast-enhancing properties of albumin-(Gd-DTPA) and Gd-DTPA at 2.0 T: and experimental study in rats. AJR Am J Roentgenol 1986;147:1263–1270.
30. Caravan P, Ellison JJ, McMurry TJ, Lauffer RB. Gadolinium(III) chelates as MRI contrast agents: structure, dynamics, and applications. Chem Rev 1999;99:2293–2352.
31. Larose E, Kinlay S, Selwyn AP, Yeghiazarians Y, Yucel EK, Kacher DF, Libby P, Ganz P. Improved characterization of atherosclerotic plaques by gadolinium contrast during intravascular magnetic resonance imaging of human arteries. Atherosclerosis 2008;196:919–925.
32. Bloembergen N, Purcell EM, Pound RV. Relaxation effects in nuclear magnetic resonance absorption. Phys Rev 1947;73:679–712.
33. Caravan P, Cloutier NJ, Greenfield MT, McDermid SA, Dunham SU, Bulte JW, Amedio JC, Jr., Looby RJ, Supkowski RM, Horrocks WD, Jr., McMurry TJ, Lauffer RB. The interaction of MS-325 with human serum albumin and its effect on proton relaxation rates. J Am Chem Soc 2002;124:3152–3162.
34. Kobayashi H, Kawamoto S, Jo SK, Bryant HL, Jr., Brechbiel MW, Star RA. Macromolecular MRI contrast agents with small dendrimers: pharmacokinetic differences between sizes and cores. Bioconjug Chem 2003;14:388–394.